Insight into the Structure of Layered Zinc Hydroxide Salts Intercalated with Dodecyl Sulfate Anions

ARTICLE *in* THE JOURNAL OF PHYSICAL CHEMISTRY C · NOVEMBER 2014

Impact Factor: 4.77 · DOI: 10.1021/jp508499g

8 AUTHORS, INCLUDING:

Jan Demel
Academy of Sciences of the Czech Republic
24 PUBLICATIONS **356** CITATIONS
SEE PROFILE

Kamil Lang
Academy of Sciences of the Czech Republic
137 PUBLICATIONS **2,470** CITATIONS
SEE PROFILE

THE JOURNAL OF PHYSICAL CHEMISTRY C

Article

pubs.acs.org/JPCC

Insight into the Structure of Layered Zinc Hydroxide Salts Intercalated with Dodecyl Sulfate Anions

Jan Demel,[†] Jan Hynek,[†] Petr Kovář,[‡] Yan Dai,[§] Christine Taviot-Guého,[§] Ondřej Demel,[∥] Miroslav Pospíšil,[‡] and Kamil Lang*,[†]

[†]Institute of Inorganic Chemistry of the Academy of Sciences of the Czech Republic, v.v.i., Husinec-Řež 1001, 250 68 Řež, Czech Republic

[‡]Faculty of Mathematics and Physics, Charles University in Prague, Ke Karlovu 3, 121 16 Praha, Czech Republic

[§]Institut de Chimie de Clermont-Ferrand, UMR-CNRS no. 6296, Université Blaise Pascal, BP 80026, 63177 Aubière Cedex, France

[∥]J. Heyrovský Institute of Physical Chemistry of the Academy of Sciences of the Czech Republic, v.v.i., Dolejškova 3, 182 23 Praha, Czech Republic

Supporting Information

ABSTRACT: This Article presents the systematic experimental and theoretical investigation of the structural arrangements of dodecyl sulfate (DS) anions in the interlayer space of layered zinc hydroxide salts (LZH-DS) and of the structure of zinc hydroxide layers, with a detailed description of the zinc ions' coordination environment. As-prepared, well-crystalline LZH-DS has a basal spacing of 31.5 Å. After treatment with methanol at room temperature, zinc hydroxide layers shrank to form two new layered phases with basal spacings of 26.4 and 24.7 Å. The shrinking was accompanied by a decrease in the content of DS anions in the interlayer space, indicating a change in the alignment of the intercalated anions and a decrease in the charge density of the zinc hydroxide layers. The latter effect was assessed by the atomic pair distribution function (PDF) analysis of powder X-ray diffraction patterns, revealing the successive removal of Zn ion tetrahedra from the hydroxide layers, with the octahedrally coordinated Zn ions left unaffected. The interlayer space of all three phases was modeled by molecular dynamics, and the models were validated by the comparison of modeled and experimental powder XRD patterns and one-dimensional electron density maps. The arrangement of DS anions in the interlayer space of LZH-DS also depended on temperature. Remarkably, the basal spacing was considerably increased at 55 °C, which was explained by the formation of a second-staging heterostructure with the regular alternation of layers with two basal spacings, 31.5 and 34.2 Å. This is the first reported interstratification phenomenon in layered hydroxides intercalated with aliphatic molecules. Our results provide insight into the great variability of layered hydroxide structures controlled by external stimuli.

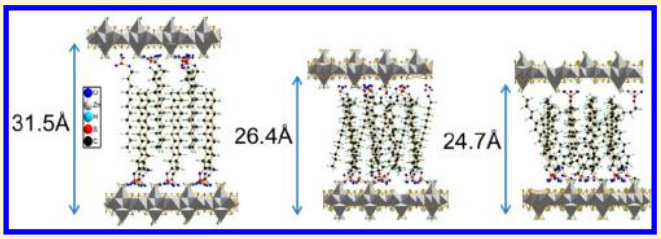

INTRODUCTION

Layered hydroxides are two-dimensional layered materials composed of positively charged brucite-like layers with anions intercalated in the interlayer space. The structures most often studied are layered double hydroxides (LDH) of the general formula $[M^{2+}_{1-x}M^{3+}_{x}(OH)_2]^{x+}[A^{n-}]_{x/n}\cdot mH_2O$, where M^{2+} = Mg^{2+}, Zn^{2+}, Co^{2+}, Ni^{2+}, etc.; M^{3+} = Al^{3+}, Fe^{3+}, Co^{3+}, etc.; and A^{n-} is the intercalated anion, which can vary from a simple inorganic to a targeted organic anion introducing a synergistic functionality to this organic/inorganic hybrid. The distance between inorganic hydroxide layers depends on the size and arrangement of the intercalated anions.[1,2]

In recent years, extensive research has been devoted to studying layered simple hydroxides that contain a single type of metal cation with a positive charge created by hydroxyl vacancies.[3−5] The representative hydroxides are $M_2(OH)_3(A^{n-})_{1/n}\cdot mH_2O$ (M = Co^{2+}, Cu^{2+}, Ni^{2+}) or layered zinc hydroxide salts $Zn_5(OH)_8(A^{n-})_{2/n}\cdot 2H_2O$ (LZHs). In the hydroxide layers of LZHs, one-quarter of octahedrally coordinated zinc ions are replaced by two tetrahedrally coordinated zinc ions located below and above the plane, with water molecules coordinated at the apexes of the tetrahedra.[6] LZHs are widely used as inorganic matrixes for the encapsulation of anionic dyes[7−9] and drugs,[10,11] and as precursors for the preparation of ZnO sheets[12] or nanosheets.[13−15] These applications require the intercalation of a variety of functional anions.

The properties of layered hydroxides depend on the composition and structure of the host layers and on the composition of the interlayer space. Information regarding the conformation and binding properties of intercalated anions allows for the assessment of structure−property relationships. The binding modes of anion−host interactions vary from diffuse electrostatic interactions in LDHs to coordination

Received: August 22, 2014
Revised: October 24, 2014
Published: October 24, 2014

monodentate interactions in layered copper hydroxides[16] with the variety of anion conformations caused by temperature or air humidity.[17] Because of their layered structure, LDHs and LZHs are usually poorly crystalline materials due to stacking faults, turbostraticity, and interstratification, rendering the description of the structure and related properties of these materials difficult. Therefore, in this respect, a multitool approach utilizing advanced computational and experimental methods is required. Molecular dynamics simulations and DFT calculations have been used to propose an interlayer structure and the changes it undergoes under varying conditions.[7,18−23] The analysis of the peak intensity of the (h00) plane obtained by powder X-ray diffraction can help to develop structural models of the interlayer space by the calculation of a one-dimensional electron density distribution along the a-stacking axis. Finally, the pair distribution functions (PDFs) obtained by the Fourier transformation of the entire X-ray scattering pattern can be used to provide details regarding the local structure of the hydroxide layers.[24−27]

The direct precipitation of Zn^{2+} by NaOH in the presence of dodecyl sulfate (DS) anions leads to LZH intercalated with DS (LZH-DS). The layered structure has a basal spacing of 31.5 Å, and thus the produced material is hereafter referred to as LZH-DS_{ex}. In our previous study, we described the minor formation of a second phase with a basal spacing of approximately 26.4 Å.[13] This new phase appeared when the molar ratio of DS/Zn^{2+} in the reaction mixture was above 1.9. The formation of two LZH phases was also reported by Miao et al. for LZH-benzoate prepared by precipitation in alcohols; however, no structural analysis was provided.[28]

In this Article, we describe, for the first time, the synthesis of three phases of LZH-DS. A detailed analysis of powder X-ray diffraction data, including both Bragg peaks and diffuse scattering, combined with molecular modeling and DFT calculations allowed us to describe the structure of the hydroxide layers and the arrangement of dodecyl sulfate molecules located in the interlayer space. Upon gentle thermal treatment of the extended LZH-DS_{ex} phase, we observed interlayer expansion accompanied by interstratification. The phenomenon of interstratification[29] or second staging, that is, the periodical alternation of interlayers with different basal spacings, is rarely observed for layered hydroxides, and, in most cases, the interstratification is induced by intercalation with two different anions in the neighboring interlayers.[30,31] Examples of second staging induced by relative humidity[32] or temperature[33] are even rarer. The existence of the three LZH-DS phases and the second staging reveal the significant effects of organic solvents, the chemical composition and charge density of the layers, and temperature on the interlayer arrangement of anions in layered hydroxides. We report that the structure and properties of layered hydroxides fabricated for specific applications can be fine-tuned by adjusting the synthesis parameters and surrounding conditions.

EXPERIMENTAL SECTION

Materials. $Zn(NO_3)_2{\cdot}6H_2O$, NaOH (both Lachner, Czech Republic), and sodium dodecyl sulfate (Sigma-Aldrich) were used as purchased. Methanol (MeOH, Penta, Czech Republic) was dried over 3 Å molecular sieves (Sigma-Aldrich).

Synthesis of Layered Zinc Hydroxide Intercalated with Dodecyl Sulfate Anion: The Extended Phase (LZH-DS_{ex}). LZH-DS_{ex} was prepared by the precipitation method described previously:[13] $Zn(NO_3)_2{\cdot}6H_2O$ (20.1 g; 67.6 mmol) and sodium dodecyl sulfate (3.03 g; 10.5 mmol) were dissolved in 200 mL of water. A total of 50 mL of 0.75 M NaOH (37.5 mmol) was added dropwise to the vigorously stirred solution during 5 h at room temperature. Immediately after the addition of NaOH, the suspension was centrifuged (Hettich Rotina 35, 7000 rpm, 4 min) and washed three times with water. The white precipitate was air-dried at room temperature.

Treatment of LZH-DS_{ex} in Organic Solvents. 0.1 g of LZH-DS_{ex} was suspended in 4 mL of organic solvent (MeOH, ethanol, 2-propanol, 1-butanol, 1-octanol, acetone, toluene, and chloroform) and shaken for 24 h (Table 1). The suspension was then filtered and washed by the given organic solvent. The white product was air-dried at room temperature.

Table 1. Basal Spacings of the LZH-DS Phases Obtained by the Treatment of LZH-DS_{ex} in Organic Solvents for 24 h at Room Temperature[a]

	extended phase		shrunk phase	
solvent	basal spacing/Å	peak area/%	basal spacing /Å	peak area/%
MeOH/4 h			26.4	100
MeOH			24.7	100
ethanol	30.5−31.4[b]	97	27.3	3
2-propanol	30.6	89	27.4	11
1-butanol	30.7	78	27.4	22
1-octanol	30.7	79	27.4	21
acetone	30.6	91	27.4	9
toluene	31.5	91	26.6−27.4[b]	9
chloroform	31.5	88	27.4	12

[a]The original basal spacing of LZH-DS_{ex} was 31.5 Å. The ratio of the respective phases was calculated as the area ratio between the corresponding 200 diffraction lines. The basal spacings were reproducible, and the estimated error of the peak area was 5%. [b]The formation of two phases with similar basal spacings was observed.

Synthesis of LZH-DS_s. 0.5 g of LZH-DS_{ex} was suspended in 20 mL of MeOH and shaken for 4 h. The suspension was then filtered and washed by MeOH. The white product was air-dried at room temperature.

Synthesis of LZH-DS_{ss}. 0.5 g of LZH-DS_{ex} was suspended in 20 mL of MeOH and shaken for 24 h. The suspension was then filtered and washed by MeOH. The white product was air-dried at room temperature.

Instrumental Methods. Powder X-ray diffraction (XRD) was performed on a PANalytical X'Pert PRO diffractometer in transmission mode. The diffractometer was equipped with a conventional Cu X-ray tube (40 kV, 30 mA), elliptic focusing mirror, 0.5° divergence slit, 0.5° antiscatter slit, and 0.02 rad Soller slit in the primary beam. A fast PIXcel linear position-sensitive detector with an antiscatter shield and a 0.02 rad Soller slit was used to detect the diffracted beam. XRD patterns were collected over the range between 1 and 88° (2θ) with a step size of 0.0065° and an acquisition time of 510 s per step. In situ high-temperature XRD patterns were collected using a high-temperature Anton PAAR HTK-16 chamber installed on the PANalytical X'Pert PRO X-ray diffractometer (Co K_α radiation, 40 kV, 30 mA, multichannel detector X'Celerator with an antiscatter shield). For the measurement of the interstratified phase at low angles, temperature-dependent XRD patterns were recorded with a Rigaku SmartLab 3 kW diffractometer equipped with a Cu X-ray tube and high-temperature chamber TTK 450. In both cases, the measure-

dx.doi.org/10.1021/jp508499g | J. Phys. Chem. C 2014, 118, 27131−27141

ments were performed in the Bragg−Brentano geometry, and the temperature was varied from 25 to 100 °C with a step size of 5 °C. Qualitative analysis was performed with the HighScorePlus software package (PANalytical, Almelo, The Netherlands, version 3.0) and the JCPDS PDF-2 database.[34]

The one-dimensional (1D) electron density distribution along the *a*-stacking axis was calculated from the intensity of the *h*00 diffraction lines according to the following equation:

$$\rho(x) = \sum_{h=0}^{\infty} F_{h00} \cos\left(\frac{2\pi h x}{a}\right)$$

where a is the unit cell parameter, x is the fractional coordinate along the *a*-stacking axis, and F_{h00} are the structure factors of the *h*00 diffractions. Ten isolated *h*00 diffraction lines were used to calculate the 1D plot for LZH-DS_{ex} with a basal spacing of $d_{200} \approx 31.5$ Å and eight *h*00 diffraction lines for LZH-DS_s with a basal spacing of $d_{200} \approx 26.4$ Å. First, the Le Bail method, consisting of the refinement of the total envelope of the XRD patterns, was used to determine cell parameters assuming $C2/m$ space group symmetry, that is, the same space group symmetry of pristine layered zinc hydroxide nitrate $Zn_5(OH)_8(NO_3)_2 \cdot 2H_2O$ (LZH-NO_3), and to extract the intensities of diffraction peaks. The hydroxide part of the structure was then entered and the F_{h00} structure factors calculated; the signs of the structure factors were directly obtained from the scattering contributions of the LZH hydroxide layers assuming a relatively small contribution of the intercalated molecules. The treatment of the XRD data was carried out using the FullProf suite program.[35,36]

The pair distribution functions (PDFs) were obtained from X-ray scattering experiments using a PANalytical X'Pert Pro X-ray powder diffractometer (Bragg−Brentano $\theta-\theta$ geometry) equipped with an X'Celerator Scientific detector and Ag anticathode ($K\alpha_1 = 0.5594$ Å, $K\alpha_2 = 0.5608$ Å). The data were recorded over the range 2−130° (2θ) using variable divergence slits with a constant irradiated sample length of 10 mm and a step size of 0.01671°. The corresponding accessible maximum scattering vector Q magnitude was 20 $Å^{-1}$, although 15 $Å^{-1}$ was used as a cutoff value during the PDF analysis. To ensure good scattering statistics and a high signal-to-noise ratio, several frames were collected, resulting in an overall exposure time of 48 h. The summation of the patterns and their conversion to corresponding 0.03° pseudofixed-slit data were performed using the PANalytical X'Pert HighScore Plus software. Air scattering was taken into account by measuring the empty diffractometer background. The data were normalized and Fourier transformed to the PDF $G(r)$ using the software PDFgetX2.[37] PDF refinement was carried out using the program PDFgui.[38]

Thermal analyses (TGA/DTA/MS) were carried out using a Setaram SETSYS Evolution-16-MS instrument coupled with a mass spectroscopy system. The measurements were performed in synthetic air at a heating rate of 5 °C min^{-1}. Fourier transform infrared spectra (FTIR) were collected on a Nicolet NEXUS 670-FT spectrometer in KBr pellets. Elemental analyses were performed on a Horiba EMIA-320 V2 combustion analyzer.

Molecular mechanics and classical molecular dynamics calculations were carried out in the Cerius2 and Materials Studio modeling environments.[39] The structure of DS anions was optimized using the quantum chemistry computational program Turbomole v5.9, yielding a distance of approximately 20.3 Å between the most distant SO_3 oxygen atom and the last H atom of the DS chain, taking into account the van der Waals radii. The hydroxide layers of the cell were built from the bilayer structure in the $C2/m$ space group symmetry reported for LZH-NO_3, with both octahedrally and tetrahedrally coordinated zinc atoms leading to the following complex formula for the hydroxide layer: $[Zn^{octa}{}_3Zn^{tetra}{}_2(OH)_8(H_2O)_2]^{2+}$.[6] In this structure, one-quarter of the octahedral sites of the brucite-like layer are vacant, and tetrahedrally coordinated zinc atoms are located above and below these empty octahedral sites. The zinc tetrahedra share three corners with the octahedral layer, and the fourth one is occupied by a water molecule.

The cell parameters of LZH-DS_{ex} and LZH-DS_s were obtained by the full pattern matching refinement (FullProf suite program) of the experimental XRD patterns (see below). The simulation cell consisted of a $1 \times 2 \times 4$ structure, that is, eight monoclinic unit cells containing two zinc hydroxide layers. Thus, the formula of the hydroxide layer of LZH-DS_{ex} is $[Zn_{80}(OH)_{128}(H_2O)_{32}]^{32+} = [Zn^{octa}{}_{48}Zn^{tetra}{}_{32}(OH)_{128}(H_2O)_{32}]^{32+}$, bearing a positive electrical charge of +32 with in-plane lattice parameters $B = 12.4394$ Å and $C = 21.964$ Å.

On the basis of our experimental data, we created three structural models: (a) The model of LZH-DS_{ex} with a basal spacing of 31.5 Å ($d_{200} = a/2$) corresponds to the complete saturation of the layer charge by DS anions in the interlayer space. (b) The model of LZH-DS_s has a basal spacing of 26.4 Å, and the layer charge is reduced by 25% relative to that of LZH-DS_{ex}, in agreement with elemental analysis. The hydroxide layer was modified by the random deletion of four Zn tetrahedra located above or below the octahedral plane to yield a layer composition of $[Zn_{76}(OH)_{128}(H_2O)_{28}]^{24+}$. The decrease in the layer charge was accompanied by the removal of eight DS anions and by the placement of a hydrogen ion at one of the three hydroxyl groups previously bonded to zinc ion at four sites. (c) The model of LZH-DS_{ss} has a basal spacing of 24.7 Å, with the layer charge reduced by 31% with respect to that of LZH-DS_{ex}, in agreement with the results of elemental analysis (Table S1 in the Supporting Information). The original layer of LZH-DS_{ex} was modified by the random deletion of five zinc tetrahedra, analogously to the previous case, corresponding to an approximately 31% charge reduction and a $[Zn_{75}(OH)_{128}(H_2O)_{27}]^{22+}$ layer composition. To verify the plausibility of the interlayer arrangements, molecular dynamics calculations were also carried out with variable cell parameters, which led to layered structures with basal spacings of 31.0, 26.5, and 24.5 Å for LZH-DS_{ex}, LZH-DS_s, and LZH-DS_{ss}, respectively, corresponding well to the experimental values (31.5, 26.4, and 24.7 Å).

In all cases, the space group was set to $P1$ and the charges were calculated using the Q_{eq} method (charge equilibrium approach).[40] The models were optimized in the Dreiding force field;[41] the electrostatic energy and van der Waals energy were calculated by the Ewald summation method.[42] The structure of the hydroxide layers was kept fixed, except for the hydrogen atoms of the OH groups and water molecules at the apexes of the Zn tetrahedra. All atomic positions in the interlayer space were allowed to vary. The dynamics simulations were carried out in an NVT statistical ensemble (N, constant number of atoms; V, constant volume; T, constant temperature) at 300 K. One dynamic step was 0.001 ps, and dynamic calculations for a total period of 200 ps were carried out. All positions of the DS atoms were allowed to vary during quench dynamics. After

dx.doi.org/10.1021/jp508499g | J. Phys. Chem. C 2014, 118, 27131−27141

quench dynamics, the interlayer space of selected optimized structures was minimized to obtain the final structural models.

The longitudinal axes of DS were calculated for LZH-DS_{ex} and LZH-DS_s with nearly linear alkyl chains. The axes were taken as lines connecting the first and last carbon atoms. Because LZH-DS_{ss} has significantly distorted alkyl chains, the alkyl chains were divided into the linear parts of relative l_i lengths to collect each individual angle between the layer normal and the longitudinal axis. The resulting tilting angle was the weighted average of the individual tilting angles.

Periodic hybride Gaussian and plane wave DFT[43,44] calculations of electron density were performed using the CP2K package[45] for all three model structures. The standard Becke–Lee–Yang–Parr (BLYP) functional was used.[46,47] The Goedecker–Teter–Hutter (GTH) effective core pseudopotentials[48,49] with the DZVP-MOLOPT-SR-GTH basis set for zinc and the TZV2P-GTH basis set for the remaining elements were employed.[50] Single point calculations were performed at zero temperature using the geometries obtained from molecular dynamics simulations described above.

RESULTS AND DISCUSSION

Characterization of the Prepared Materials. Parent LZH-DS_{ex} was synthesized by direct precipitation, consisting of the slow addition of sodium hydroxide into a solution of zinc nitrate and sodium dodecyl sulfate, as described previously.[13] The composition, estimated by elemental and TGA/DTA analyses, was $Zn_5(OH)_8(DS)_2{\cdot}2H_2O$ (Table S1 in the Supporting Information). The powder X-ray diffraction pattern presented in Figure 1 is typical of layered compounds with

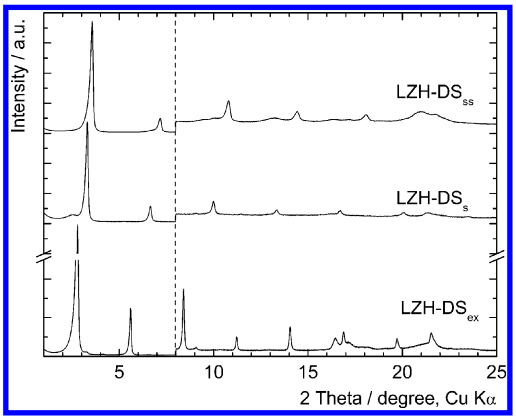

Figure 1. XRD patterns of LZH-DS_{ex} (bottom), LZH-DS_s (middle), and LZH-DS_{ss} (top). The diffractograms are vertically shifted, and the intensities above 8° (2θ) were multiplied by 10 for better clarity.

intense basal diffraction lines at low 2θ angles, whose positions depend on the size of the intercalated species. All of the observed diffraction lines could be indexed to a monoclinic cell with $C2/m$ space group symmetry as reported for pristine LZH-NO_3.[6] The sharp features of $h00$ basal diffraction lines at low 2θ angles (2θ < 20°) as compared to the asymmetric broadening of $h0l/hk0$ diffraction peaks in the mid-2θ region indicate an ordered stacking of the hydroxide layers along the a-axes and, at the same time, stacking defects or turbostratic disorders in the perpendicular directions. The cell parameters determined using the Le Bail whole powder pattern decomposition method (Figure S1A in the Supporting Information) were a = 62.950(4) Å, b = 6.2197(4) Å, c = 5.4908(3) Å, β = 92.996(4)° with a resulting basal spacing of approximately $d_{200} \approx a/2$ = 31.5 Å. Because the length of the DS chain was approximately 20.3 Å and we assumed a perpendicular orientation for the long axis of the DS alkyl chain with respect to the hydroxide layers, the basal spacing of 31.5 Å indicates interpenetration of the alkyl chains interacting with the adjacent hydroxide layers. In fact, variations in the alignment of the DS chains in the interlayer space, variations in the amount of intercalated water, and the flexibility of the DS chains may affect the resulting basal spacing. Thus, we investigated the treatment of LZH-DS_{ex} with organic solvents of different polarities to establish the effects of the respective solvents on the alignment of DS ions.

The treatment of LZH-DS_{ex} with organic solvents had a considerable effect on the basal spacing of the layered structure (Table 1). We observed the transformation of the parent LZH-DS_{ex} into two distinct layered phases. One phase, called the shrunk phase, was characterized by a basal spacing ranging between 26.4 and 27.4 Å. In MeOH, this shrunk phase (abbreviated hereafter as LZH-DS_s) showed a basal spacing of 26.4 Å, and the conversion was completed in 4 h. In other solvents, only a partial transformation up to 22% took place even after treatment for 24 h. When the 24 h treatment was applied in MeOH, the formation of an extremely shrunk phase with a basal spacing of 24.7 Å, denoted as LZH-DS_{ss}, was observed. The existence of this phase has never been reported. The occurrence of the LZH-DS_s and LZH-DS_{ss} phases suggests a complex interplay between the effects of solvent polarity, intercalated DS anions, and the OH groups of the zinc hydroxide layers on the interpenetrability of adjacent DS chains in the interlayer space.

Because both new phases, LZH-DS_s and LZH-DS_{ss}, were formed only in MeOH, the effects of MeOH were studied in detail. The empirical formulas estimated by elemental analyses (C and S by a combustion technique) were $Zn_{4.75}(OH)_8(DS)_{1.50}{\cdot}1.75H_2O$ and $Zn_{4.66}(OH)_8(DS)_{1.33}{\cdot}1.66H_2O$ for LZH-DS_s and LZH-DS_{ss}, respectively (Table S1 in the Supporting Information). Thus, the elemental analyses indicated that the amount of intercalated DS anions gradually decreases in the series LZH-DS_{ex} > LZH-DS_s > LZH-DS_{ss}, that is, by approximately 25% and 33% for LZH-DS_s and LZH-DS_{ss}, respectively, as compared to that of the parent LZH-DS_{ex}. As proposed below, the drop in the DS content is caused by the removal of some Zn tetrahedral cations from the hydroxide layers, accompanied by a reduction in the layer charge density. The mass spectroscopy measurement of the methanol supernatant revealed peaks of m/z 265.3, 859.7, and 1457.3 attributed to DS^-, $Zn(DS)_3^-$, and $Zn_2(DS)_5^-$, respectively, confirming that zinc cations and DS anions leach out in the form of $Zn(DS)_2$.[13]

The cell parameters determined by the Le Bail method for LZH-DS_s were a = 52.820(5) Å, b = 6.2258(6) Å, c = 5.4891(4) Å, β = 91.774(2)°, and the resulting basal spacing was approximately $d_{200} \approx a/2$ = 26.4 Å (Figure S1B in the Supporting Information). On the other hand, the decrease in the crystallinity of LZH-DS_{ss} did not allow for whole powder pattern decomposition and therefore did not allow for the cell parameters to be determined exactly. The basal spacing for LZH-DS_{ss} was estimated from the position of the first $h00$ harmonic, leading to a value of $d_{200} \approx$ 24.7 Å. The positions of the nonbasal diffraction lines were rather similar in all three phases, suggesting that the hydroxide layers possessed a

dx.doi.org/10.1021/jp508499g | J. Phys. Chem. C 2014, 118, 27131–27141

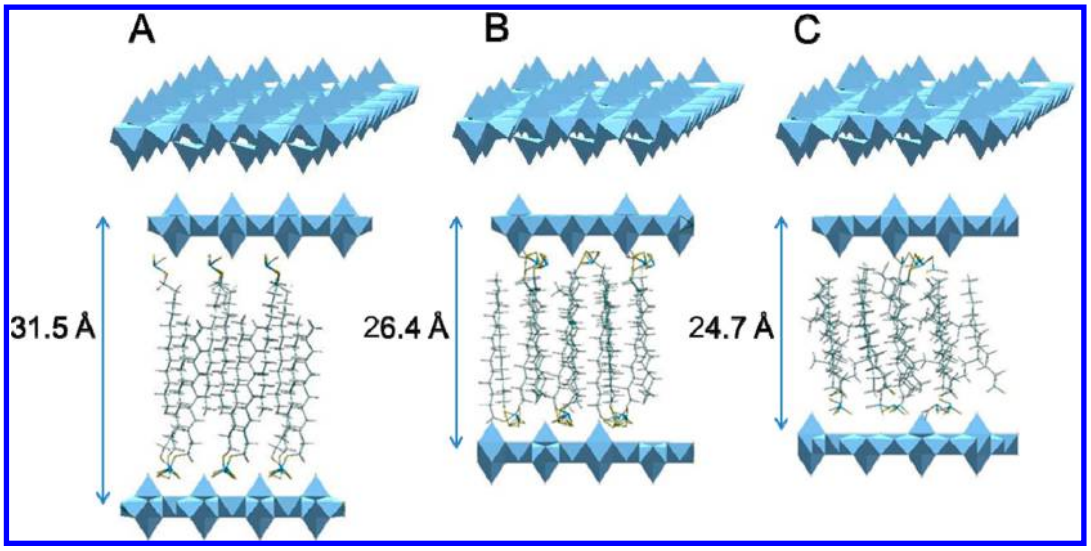

Figure 2. Molecular dynamics simulations of the interlayer space of (A) LZH-DS_{ex}, (B) LZH-DS_s, and (C) LZH-DS_{ss}.

structure similar to that of the original zinc hydroxide layers of pristine LZH-NO_3.

The thermal behavior of the phases showed features similar to those of other layered zinc hydroxides (Figures S2, S3, S4 in the Supporting Information).[13] The first endothermic process, up to approximately 130 °C, corresponds to the release of structural water molecules and the partial dehydroxylation of the hydroxide layers, as determined by the mass spectroscopy of gas products, mass balance, and in situ high-temperature XRD documenting the decomposition of the layered structure at approximately 130 °C. The onset of CO_2 release, indicating the thermal decomposition of the alkyl chains, occurred at approximately 150 °C and was accompanied by the complete dehydroxylation of the layers. The main portion of sulfur was released above 800 °C. The main difference among the phases was the total mass loss, which was 59.4%, 54.2%, and 53.1% for LZH-DS_{ex}, LZH-DS_s, and LZH-DS_{ss}, respectively, corresponding well with the estimated empirical formulas.

The FTIR spectra of all three phases were the same and displayed the vibrations of intercalated DS anions and water molecules (OH stretching vibrations at approximately 3500 cm^{-1} and OH deformation vibrations at 1630 cm^{-1}) (Figure S5 in the Supporting Information). The spectra are dominated by bands associated with C−H stretching vibrations at approximately 2850, 2920, and 2956 cm^{-1}. The bands of the sulfate group are shifted to lower frequencies relative to those observed for sodium dodecyl sulfate (ν_{as} 1219 and 1251, ν_s 1084 cm^{-1}; LZH-DS: ν_{as} ~1220 (broad), ν_s 1062 cm^{-1}).

Structural Arrangement of the Interlayer Space. Molecular dynamics simulations allowed for the reconstruction of the alignment of the intercalated molecules. The optimized structure of the LZH-DS_{ex} interlayer space, depicted in Figure 2A, indicates a good match between the calculated and measured XRD patterns (Figure 3). Additionally, the agreement between the observed and calculated intensities of the (h00) planes is quite good, confirming the atomic content of these planes. Evidently, DS anions adopt an ordered bilayer structure composed of interpenetrating alkyl chains, with the longitudinal axis nearly perpendicular to the host hydroxide layers and with oxygen atoms of the SO_3^- groups located approximately in the plane with oxygen atoms of the water molecules that are attached to the apexes of tetrahedral zinc

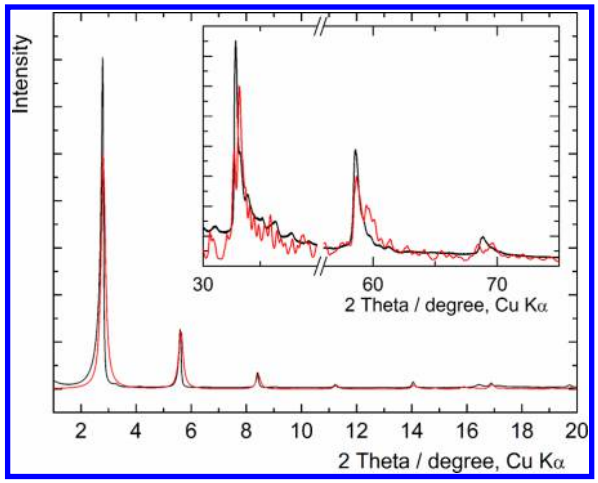

Figure 3. Comparison of the experimental powder XRD pattern of LZH-DS_{ex} (black line) with the XRD pattern obtained by molecular dynamics (red line). Inset: Detail of the nonbasal diffraction lines.

cations (Figure 4). The regular ordering of DS anions can be related to the distribution of the free space in the interlayer cell volume: the overall filled space of the cell is 65% with the free cell volume[51] located mainly between the chain ends and the

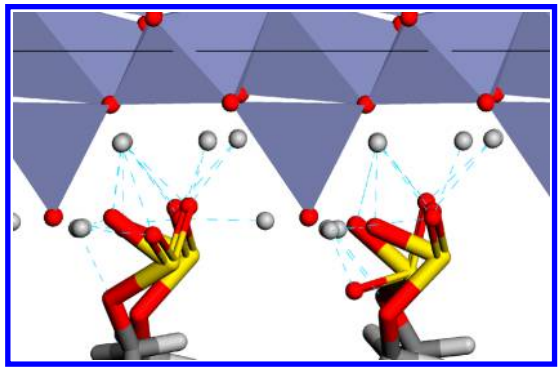

Figure 4. Hydrogen-bonding pattern in LZH-DS_{ex} between the sulfate groups of DS ions and hydrogen atoms (light gray balls) of the zinc hydroxide layer.

dx.doi.org/10.1021/jp508499g | J. Phys. Chem. C 2014, 118, 27131−27141

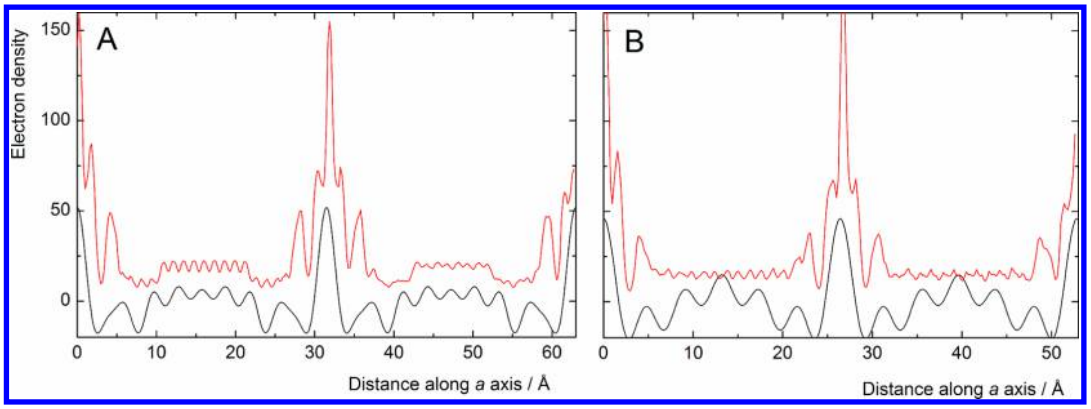

Figure 5. Comparison of 1D electron density maps of (A) LZH-DS_{ex} and (B) LZH-DS_s calculated from the XRD patterns (black) and obtained by the DFT analysis of the molecular dynamics simulation models (red).

host layers due to the vertical shift of the guests. The middle part of the interlayer space with the interpenetrated alkyl chains is filled from 85%, resulting in a very low variability of the guest location. The ordered chain arrangement is also demonstrated in the top view of the interlayer space (Figure S6 in the Supporting Information). The average distance between neighboring DS chains is approximately 4 Å.

The amount of DS anions in the interlayer space of the LZH-DS_s and LZH-DS_{ss} models was set 25% and 31% lower than that in the LZH-DS_{ex} phase, respectively (Table S1 in the Supporting Information). The calculated occupied cell volumes were very similar to the occupied cell volume of LZH-DS_{ex} and were 62% and 63% for LZH-DS_s and LZH-DS_{ss}, respectively. However, the free volumes were more evenly distributed. The space filling in the area of the overlapping alkyl chains was approximately 70%, which led to larger average distances between DS chains of approximately 5 Å and a large variability in chain tilting and deformation.

In LZH-DS_s, the major part of the DS chains is nearly perpendicular to the host layers, with tilting angles between 0° and 15° and an average of approximately 8° (Figure 2B). This model well reproduces the experimental powder XRD pattern at low angles; the calculated pattern is better resolved in the region of nonbasal diffractions not addressing the defects present in the real samples (Figure S7 in the Supporting Information). In the case of LZH-DS_{ss}, the gallery size (19.3 Å) is even smaller than the van der Waals length of the DS chain (20.3 Å), which results in a tilting of DS with an average angle of approximately 24°. Because of the flexibility of DS anions and the repulsive interactions between the hydrophobic alkyl chains and the hydroxide layers, the DS chains are likely to be more distorted, causing structural disorder in the interlayer space (Figure 2C), which may explain the lower crystallinity of the sample. The experimental and calculated XRD patterns are well superimposed, similarly to those obtained for LZH-DS_s (Figure S8 in the Supporting Information).

The number of *h*00 harmonics observed in the XRD patterns of LZH-DS_{ex} and LZH-DS_s enabled the calculation of the 1D electron density distribution along the *a*-stacking axis for these two compounds, as shown in Figure 5. This calculation was not possible for LZH-DS_{ss} due to the lower crystallinity of this phase. To better understand these experimental 1D plots, the theoretical 1D plot for LZH-NO_3 was also calculated for the experimental structure reported by Stählin et al.[6] (Figure S9 in the Supporting Information). The 1D electron density map of LZH-NO_3 displays two strong maxima at 0 and 9.7 Å corresponding to the metal-containing hydroxide layers. The peak on each side arises from zinc ions in the tetrahedral coordination above and below the octahedrally coordinated zinc ions. Nitrate anions produce two maxima in the interlayer space at approximately 4.2 and 5.6 Å from the center of the hydroxide layers, which is consistent with the anions' regular arrangement and hydrogen-bonding interactions between nitrate anions and the bonded water and OH groups of the layers.

In LZH-DS_{ex} and LZH-DS_s, the most intense peaks calculated from the XRD patterns correspond to the electron densities of zinc hydroxide layers (Figure 5). The distances between two successive maxima are equal to the basal spacings, that is, 31.5 and 26.4 Å for LZH-DS_{ex} and LZH-DS_s, respectively. The 1D maps obtained by DFT calculations of the modeled structures show clearly distinguishable tetrahedrally coordinated zinc ions that are not resolved in the experimental maps. The sulfate groups and apical water molecules are responsible for the nearest maxima located in the outer parts of the interlayer space near the hydroxide layers. The locations of these maxima deviate from those shown in the experimental maps as a result of the degree of freedom of DS atoms in voids close to the layers. The electron density plateaus located in the middle of the interlayer space arise from the alkyl chains of DS molecules. Although the modeled maps represent static electron densities with the thermal atomic movement omitted, these maps are consistent with the experimental densities.

Interstratification and Structural Arrangement of the Interlayer Space. The thermal treatment of LZH-DS_{ex}, monitored by in situ high-temperature XRD, led to the formation of other new phases and expanded the rich intercalation chemistry of this layered material (Figures 6 and 8, Figure S10 in the Supporting Information). At 55 °C, *h*00 diffraction lines clearly moved to lower 2θ values, with additional diffraction lines appearing at 4.1°, 6.8°, 9.5°, etc. (2θ), indicating an expansion of the interlayer space. The position of the first line of the *h*00 series located at 2.7° (2θ) yields a basal spacing of 32.8 Å. However, to determine all *h*00 harmonics, one must consider a basal spacing of 65.7 Å with a diffraction line expected at a 2θ angle of 1.35° (2θ) for the first *h*00 harmonic, which is therefore not measurable under the experimental conditions applied. If one considers that the basal spacing is 65.7 Å, then the second harmonic is expected at 32.8 Å (2*h*00), the third at 21.9 Å, the fourth at 16.4 Å, and the fifth at 13.1 Å, which exactly correspond to the XRD peaks

dx.doi.org/10.1021/jp508499g | J. Phys. Chem. C 2014, 118, 27131−27141

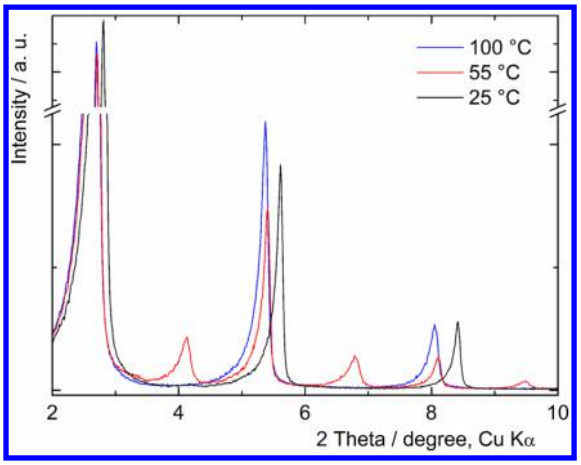

Figure 6. Temperature evolution of the XRD patterns of LZH-DS_{ex} recorded at room temperature (25 °C), 55 °C (interstratified phase), and 100 °C (temperature-extended phase).

observed. Because TGA/DTA analysis proves that no decomposition of the zinc hydroxide layers and DS anions occurs at 55 °C (Figure S2 in the Supporting Information), such an unexpected evolution of the XRD pattern has to be attributed to a temperature-induced rearrangement of the alkyl chains in the interlayer space. It is in accordance with the behavior of LDH−stearate and LDH−oleate intercalation compounds showing that the intercalated long aliphatic chains can undergo temperature-induced phase transitions connected with the increase of the basal spacing.[52]

At 65 °C, the observed additional peaks disappeared, and the remaining peaks can be explained by considering only a phase with a basal spacing of 32.8 Å (Figure 6). One may expect the removal of interlayer water molecules; however, this removal generally results in a decrease in the basal spacing[19] and not an increase, as observed in this study, by approximately Δd = +1.3 Å relative to the basal spacing of the original LZH-DS_{ex}. Upon cooling from 70 °C to room temperature, the basal spacing of the extended phase contracts from 32.8 to 31.0 Å. The difference between the heated-cooled (31.0 Å) and original samples (31.5 Å) may indicate that the time required to reach the steady state is longer than the time required for the measurement itself. Above 130 °C, the layered structure collapses, as demonstrated by the gradual substitution of the new diffraction lines of oxide-sulfate $Zn_3(SO_4)_2O$ (JCPDS 02-1476) for the basal and nonbasal diffraction lines. Above 800 °C, the only presence of ZnO (JCPDS 36-1451) is observed. The alignments of DS anions obtained by molecular dynamics simulations in all cases described are presented in Figure 7.

The XRD pattern observed at 55 °C strongly suggests the occurrence of a staging phenomenon.[29] Indeed, as shown in Figures 7B and 8, the experimental XRD pattern is in good agreement with the XRD pattern calculated by considering the regular alternation of the layers with two basal spacings, 31.5 and 34.2 Å, leading to a total basal spacing of 65.7 Å from which all of the *h*00 harmonics observed can be explained as demonstrated above. The absence of residual parent LZH-DS_{ex}

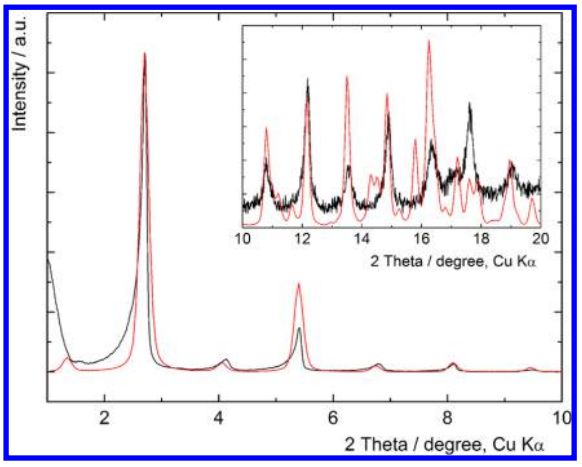

Figure 8. Comparison of the experimental (black) and calculated (red) XRD basal diffraction lines of interstratified phase recorded at 55 °C (see Figure 7B). Inset: Details of the XRD pattern between 10° and 20° (2θ).

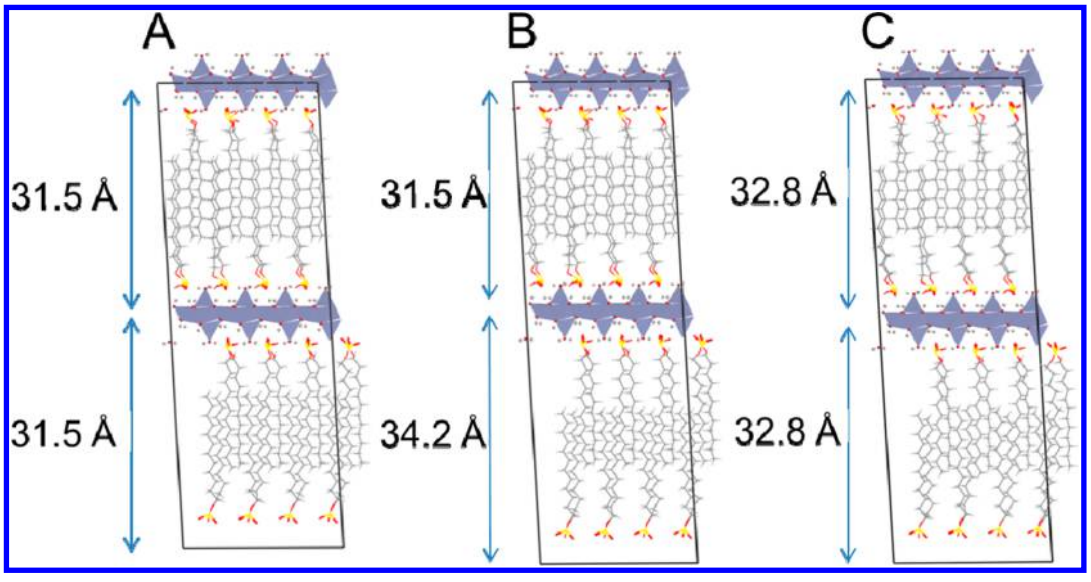

Figure 7. Molecular dynamics simulations of the interlayer space of LZH-DS_{ex} during the heat treatment: (A) starting LZH-DS_{ex} phase, (B) interstratified phase at 55 °C, and (C) temperature-extended phase at 100 °C.

dx.doi.org/10.1021/jp508499g | J. Phys. Chem. C 2014, 118, 27131−27141

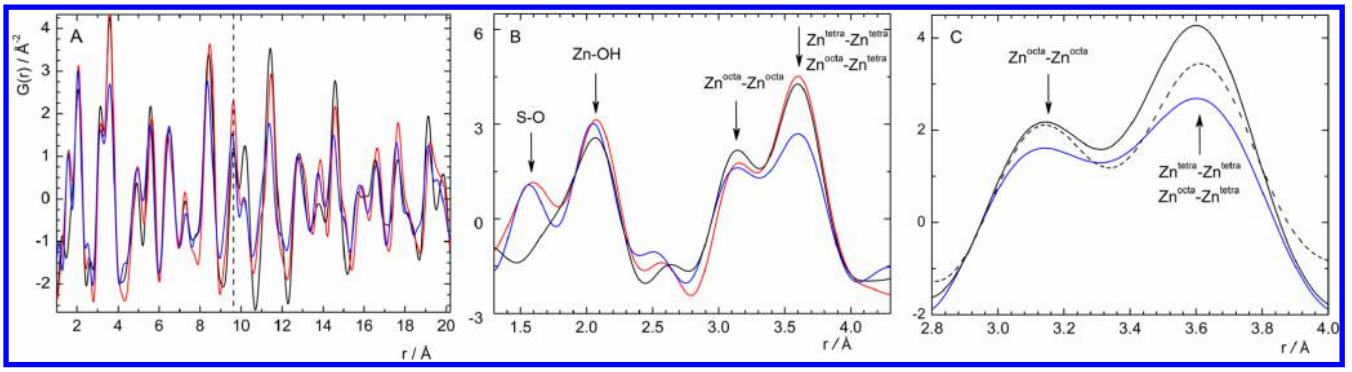

Figure 9. (A) Experimental PDFs of LZH-NO_3 (black line), LZH-DS_{ex} (red line), and LZH-DS_s (blue line). The dashed vertical line at 9.7 Å represents the basal spacing of LZH-NO_3. (B) Assignment of the PDF peaks in the range $1.5 < r < 4$ Å; LZH-NO_3 (black line), LZH-DS_{ex} (red line), LZH-DS_s (blue line). (C) Comparison of the experimental PDF of LZH-NO_3 (black line) and LZH-DS_s (blue line) to a simulated PDF of the LZH hydroxide layer (dashed black line) considering the removal of 12.5% of Zn^{tetra} atoms.

is also indicative of purity and crystallinity rarely observed for interstratified samples.

The thermal treatment of LZH-DS_s did not lead to the appearance of new diffraction lines (Figure S11 in the Supporting Information). At 55 °C, the interlayer space of LZH-DS_s began to expand, and the expansion reached a value of Δd = +1.4 Å at 65 °C, identical to that observed for LZH-DS_{ex}. These results exclude interstratification phenomena in this case.

To interpret the experimental data, we performed a set of molecular simulations and observed that the above-described transformations can be attributed to the varying degree of interpenetration of DS molecules within the interlayer space. As follows from the structural analysis, the expansion of the interlayer distance of LZH-DS_{ex} and LZH-DS_s by 1.3−1.4 Å at 65 °C corresponds to the pulling out of one CH_2 group from the interpenetrated zone of the DS chains (Figure 8A, B). For the interstratified phase obtained at 55 °C, every second interlayer space is expanded by Δd = +2.7 Å, yielding the basal spacing of 34.2 Å. The difference is roughly double the difference between the original and the 65 °C phase for both LZH-DS_{ex} and LZH-DS_s. This comparison suggests that the expansion of every second layer is caused by the pulling out of the CH_2−CH_2 parts of alkyl chains, which can be understood in terms of the layer-charge and anion size−hydrophobicity relation. The DS chains in LZH-DS_{ex} are tightly packed, and the shift caused by the CH_2−CH_2 groups is energetically more favorable than that caused by the CH_2 groups because the latter requires the substantial rearrangement of the aliphatic chains. At higher temperatures or when DS anions have more degrees of freedom, as in LZH-DS_s, the molecular system relaxes to the thermodynamically stable interlayer structure via the vertical shift of only one CH_2 group. Therefore, the interstratified compound observed at 55 °C appears to be an intermediate phase that forms before the complete relaxation of the crystal.

Structure of the Zinc Hydroxide Layers. To gain insight into the zinc ion distribution between octahedral and tetrahedral sites, PDF analysis was employed. In Figure S12A (Supporting Information), the experimental PDF of LZH-NO_3 and the PDF calculated from the structural model reported by Stählin et al.[6] are compared. The quality of the experimental data allowed a refinement of the PDF over the range $1.5 < r < 20$ Å starting from the structural parameters proposed by Stählin et al.[6] The scale factor, the PDF peak width, the lattice parameters, the position and displacement parameters of zinc atoms were refined using the PDFgui program. The final values are listed in Supporting Information Table S2, and the graphical output of the refinement is given in Figure S12B (Supporting Information). Obviously, Stählin's model well describes the observed PDF in the range $1.5 < r < 20$ Å. This agreement also validates the experimental conditions applied here for PDF acquisition, indicating an acceptable resolution in the real space for a maximum scattering vector Q magnitude of 15 Å^{-1}.

All of the interatomic distances below 20 Å can be assigned: the first PDF peak is attributed mainly to the Zn−OH bonds in both tetrahedral (Zn3−OH: 1.93−1.96 Å) and octahedral (Zn1−OH, Zn2−OH: 2.08−2.16 Å) environments (Figure 9B). The Zn−Zn bond distances for the second coordination sphere are different for the tetrahedral (labeled Zn3 by Stählin et al.[6]) and octahedral (Zn1, Zn2) environments. Indeed, Zn−Zn distances involving either one or two Zn atoms in the tetrahedral environment are on the order of 3.4−3.6 Å, whereas Zn−Zn distances between Zn atoms in the octahedral environment are shorter, 3.1−3.2 Å, leading to a double peak in the PDF. For larger interatomic distances, peaks are assigned to several Zn−Zn, OH−OH, and Zn−OH atomic pairs as the number of possible pairs increases with the interatomic distances. Contributions of pairs of atoms belonging to the adjacent hydroxide layers (interlayer contributions) are also expected for r values above the basal spacing (i.e., 9.7 Å) (Figure 9A). Because of the low density of the interlayer space as compared to the packed structure of the hydroxide layers, the contribution of the interlayer anionic species, that is, NO_3^- anions, to the PDF is weak, as indicated in Figure S12B (Supporting Information). Because of the cutoff at a finite value of Q_{max} = 15 Å^{-1} and Fourier termination errors, it was not possible to observe the N−O distances expected at 1.2−1.3 Å according to the structural model of Stählin et al.[6]

The experimental PDFs of LZH-DS_{ex} and LZH-DS_s are compared to the PDF of LZH-NO_3 in Figure 9A. The sharp peaks observed for the two LZH-DS samples indicate rather well-defined local structure. Similarly to the LZH-NO_3 sample, a weak contribution of the interlayer species is expected due to the low X-ray scattering power of C atoms and the relatively low packing density in the interlayer region. For this reason, only the S−O bonds of the sulfate anionic groups are detected at 1.6 Å (Figure 9B). Because the interlayer distance in LZH-NO_3 is 9.7 Å, the differences observed between LZH-NO_3 and LZH-DS intercalates for $r > 9.7$ Å are due to both intra- and interlayer contributions in LZH-NO_3. On the other hand, the

dx.doi.org/10.1021/jp508499g | J. Phys. Chem. C 2014, 118, 27131−27141

differences observed between LZH-DS intercalates are only due to intralayer contributions because the basal spacings are 31.5 and 26.7 Å for LZH-DS_{ex} and LZH-DS_s, respectively.

As shown in Figure 9B, a significant decrease in the intensity of the peak centered at ~3.60 Å is observed between LZH-DS_{ex} and LZH-DS_s samples, which is attributed to a decrease in the number of tetrahedrally coordinated Zn ions in LZH-DS_s. Indeed, as indicated above, Zn−Zn pairs corresponding to the second coordination sphere of Zn ions and involving at least one Zn ion in the tetrahedral environment (Zn^{tetra}–Zn^{tetra} and Zn^{tetra}–Zn^{octa} pairs) mainly contribute to the peak at ~3.60 Å. Given the many unknowns about LZH-DS_{ex} and LZH-DS_s structures, no refinement of the experimental PDF of LZH-DS intercalates was attempted. Nevertheless, assuming the removal of 12.5% Zn^{tetra} (consistent with a reduction of the layer charge by 25%), a simulation of the zinc hydroxide layers was performed starting from the atomic positions reported for LZH-NO_3, and as can be shown in Figure 9C, a net decrease in the intensity of the peak at ~3.60 Å is obtained. Thus, the decrease in the intensity of the ~3.60 Å peak clearly indicates a decrease in the number of tetrahedrally coordinated Zn ions in LZH-DS_s relative to the number of such ions in LZH-DS_{ex}.

Two plausible models of the Zn hydroxide layer modification in LZH-DS_s are schematically shown in Figure 10: (i) Both

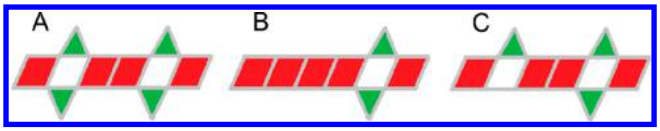

Figure 10. Schematic illustrating the structure of the zinc hydroxide layers: (A) original phase LZH-DS_{ex}, (B, C) models of LZH-DS_s.

opposite Zn^{tetra} ions are removed from the tetrahedral positions; one Zn ion takes away both opposite DS anions to form $Zn(DS)_2$ and one Zn ion fills the gap in the Zn^{octa} plane to maintain the electroneutrality of the layered structure (Figure 10B). (ii) One zinc tetrahedron and two DS anions are removed, leaving a gap in the octahedral plane (Figure 10C). Because no other differences in the PDF data were observed between the experimental PDF for $r < 9.7$ Å, in particular no modification of the intensity of the peak assigned to Zn^{octa}–Zn^{octa} atomic pairs, the second hypothesis seems to us more likely.

We show that the rearrangement of the interlayer space filled with interacting DS anions can be accompanied by structural changes in the zinc hydroxide layers. In accordance with the presented results, we propose that the LZH-DS_{ss} phase has a lower fraction of tetrahedral Zn ions in the hydroxide layers than does LZH-DS_s. All of the structures are schematically presented in Figure 2. The fact that the longer treatment of LZH-DS_{ex} by MeOH (performed up to 1 week) did not produce even tighter layered phases indicates the stability of the LZH-DS_{ss} phase. The variability of the zinc ion distribution within the hydroxide layers is a new phenomenon that may be a more general propensity of layered hydroxide salts.

CONCLUSIONS

We have described the variability in the arrangement of DS anions between the zinc hydroxide layers of the corresponding layered zinc hydroxide salt. The structures of these intercalates depend on materials treatment and temperature. The shrinking of the basal spacing, caused by the methanol treatment, is accompanied by the decreasing number of intercalated DS anions, indicating a structural change in the hydroxide layers. This behavior was confirmed by PDF analysis, which showed that the decreasing charge density of the hydroxide layers is caused by the decreasing fraction of tetrahedral Zn ions. Molecular dynamics simulations of the corresponding interlayer spaces revealed that the shrinking of the layers is accompanied by the tilting of the DS chains with respect to the layer planes and by increasing disorder.

The most extended phase, formed at 55 °C, was ascribed to the second stage intermediate, with every second hydroxide layer extended to 34.2 Å. The fact that staging behavior is favored at 55 °C for LZH-DS_{ex} can be understood in terms of the layer-charge and anion size−hydrophobicity relation. Fogg et al.[30] suggested that staging in anion-exchange intercalation reactions of LDHs proceeds via intermediates in which every second interlayer contains an exchanged guest, whereas the rest of the interlayers are filled with original anions. We describe the specific case in which the structure is filled with anions of the same type and second staging is due to the different extents of interpenetration of the DS chains. The interstratified compound was proposed to be an intermediate phase that occurs before the relaxation of the crystal. Interstratification of layered hydroxides is a rare phenomenon, and the thermal effects described herein were observed for the first time.

We show that postsynthesis treatment can have significant effects on the interlayer ordering of the anions as well as on the charge density of the hydroxide layers. We anticipate that the newly presented findings will allow for control over the structure of layered hydroxides intercalated with large functional molecules and thus facilitate tailoring hybrid materials for specific applications.

ASSOCIATED CONTENT

Supporting Information

Elemental analysis, TGA/DTA, FTIR, profile analyses of the XRD patterns, DS chain arrangement in the interlayer space, comparison of the experimental powder XRD patterns and the calculated XRD patterns, 1D plot for LZH-NO_3, in situ high-temperature XRD patterns, and PDF analysis of LZH-NO_3. This material is available free of charge via the Internet at http://pubs.acs.org.

AUTHOR INFORMATION

Corresponding Author

*Tel.: +420 26617 2193. E-mail: lang@iic.cas.cz.

Notes

The authors declare no competing financial interest.

ACKNOWLEDGMENTS

This work was supported by the Czech Science Foundation (no. 13-05114S). We thank Petr Bezdička for XRD measurements and helpful discussions. The measurement of temperature XRD by using a Rigaku SmartLab 3 kW diffractometer was carried out with the support of the core facilities of CEITEC − Central European Institute of Technology under CEITEC − open access project, ID number LM2011020.

REFERENCES

(1) Evans, D. G.; Slade, R. C. T. In *Layered Double Hydroxides (Structure and Bonding)*; Duan, X., Evans, D. G., Eds.; Springer-Verlag: Berlin, 2006; Vol. *119*, pp 1−87.

(2) Leroux, F.; Taviot-Guého, C. Fine tuning between organic and inorganic host structure: new trends in layered double hydroxide hybrid assemblies. *J. Mater. Chem.* **2005**, *15*, 3628−3642.
(3) Arizaga, G. G. C.; Satyanarayana, K. G.; Wypych, F. Layered hydroxide salts: synthesis, properties and potential applications. *Solid State Ionics* **2007**, *178*, 1143−1162.
(4) Rogez, G.; Massobrio, C.; Rabu, P.; Drillon, M. Layered hydroxide hybrid nanostructures: a route to multifunctionality. *Chem. Soc. Rev.* **2011**, *40*, 1031−1058.
(5) Demel, J.; Lang, K. Layered hydroxide−porphyrin hybrid materials: synthesis, structure, and properties. *Eur. J. Inorg. Chem.* **2012**, 5154−5164.
(6) Stählin, W.; Oswald, H. R. The crystal structure of zinc hydroxide nitrate, $Zn_5(OH)_8(NO_3)_2{\cdot}2H_2O$. *Acta Crystallogr.* **1970**, *B26*, 860−863.
(7) Demel, J.; Kubát, P.; Jirka, I.; Kovář, P.; Pospíšil, M.; Lang, K. Inorganic-organic hybrid materials: layered zinc hydroxide salts with intercalated porphyrin sensitizers. *J. Phys. Chem. C* **2010**, *114*, 16321−16328.
(8) Marangoni, R.; Ramos, L. P.; Wypych, F. New multifunctional materials obtained by the intercalation of anionic dyes into layered zinc hydroxide nitrate followed by dispersion into poly(vinyl alcohol) (PVA). *J. Colloid Interface Sci.* **2009**, *330*, 303−309.
(9) Zimmermann, A.; Jaerger, S.; Zawadzki, S. F.; Wypich, F. Synthetic zinc layered hydroxide salts intercalated with anionic azo dyes as fillers into high-density polyethylene composites: first insights. *J. Polym. Res.* **2013**, *20*, 224.
(10) Yang, J.-H.; Han, Y.-S.; Park, M.; Park, T.; Hwang, S.-J.; Choy, J.-H. New inorganic-based drug delivery system of indole-3-acetic acid-layered metal hydroxide nanohybrids with controlled release rate. *Chem. Mater.* **2007**, *19*, 2679−2685.
(11) Abdul Latip, A. F.; Hussein, M. Z.; Stanslas, J.; Wong, C. C.; Adnan, R. Release behavior and toxicity profiles towards A549 cell lines of ciprofloxacin from its layered zinc hydroxide intercalation compound. *Chem. Cent. J.* **2013**, *7*, 119.
(12) Inoue, S.; Fujihara, S. Liquid−liquid biphasic synthesis of layered zinc hydroxides intercalated with long-chain carboxylate ions and their conversion into ZnO nanostructures. *Inorg. Chem.* **2011**, *50*, 3605−3612.
(13) Demel, J.; Pleštil, J.; Bezdička, P.; Janda, P.; Klementová, M.; Lang, K. Layered zinc hydroxide salts: delamination, preferred orientation of hydroxide lamellae, and formation of ZnO nanodiscs. *J. Colloid Interface Sci.* **2011**, *360*, 532−539.
(14) Demel, J.; Pleštil, J.; Bezdička, P.; Janda, P.; Klementová, M.; Lang, K. Few-Layer ZnO nanosheets: preparation, properties, and films with exposed {001} facets. *J. Phys. Chem. C* **2011**, *115*, 24702−24706.
(15) Hynek, J.; Kalousek, V.; Žouželka, R.; Bezdička, P.; Dzik, P.; Rathouský, J.; Demel, J.; Lang, K. High photocatalytic activity of transparent films composed of ZnO nanosheets. *Langmuir* **2014**, *30*, 380−386.
(16) Švarcová, S.; Klementová, M.; Bezdička, P.; Śasocha, W.; Dušek, M.; Hradil, D. Synthesis and characterization of single crystals of the layered copper hydroxide acetate $Cu_2(OH)_3(CH_3COO){\cdot}H_2O$. *Cryst. Chem. Technol.* **2011**, *46*, 1051−1057.
(17) Iyi, N.; Ebina, Y.; Sasaki, T. Water-swellable MgAl-LDH (layered double hydroxide) hybrids: synthesis, characterization, and film preparation. *Langmuir* **2008**, *24*, 5591−5598.
(18) Kovář, P.; Pospíšil, M.; Káfuňková, E.; Lang, K.; Kovanda, F. Mg-Al layered double hydroxide intercalated with porphyrin anions: molecular simulations and experiments. *J. Mol. Model.* **2010**, *16*, 223−233.
(19) Káfuňková, E.; Taviot-Guého, C.; Bezdička, P.; Klementová, M.; Kovář, P.; Kubát, P.; Mosinger, J.; Pospíšil, M.; Lang, K. Porphyrins intercalated in Zn/Al and Mg/Al layered double hydroxides: properties and structural arrangement. *Chem. Mater.* **2010**, *22*, 2481−2490.
(20) Pisson, J.; Morel-Desrosiers, N.; Morel, J. P.; De Roy, A.; Leroux, F.; Taviot-Guého, C.; Malfreyt, P. Tracking the structural dynamics of hybrid layered double hydroxides. *Chem. Mater.* **2011**, *23*, 1482−1490.
(21) Zhang, H.; Xu, Z. P.; Lu, G. Q.; Smith, S. C. Intercalation of sulfonate into layered double hydroxide: comparison of simulation with experiment. *J. Phys. Chem. C* **2009**, *113*, 559−566.
(22) Yan, D.; Lu, J.; Wei, M.; Li, H.; Ma, J.; Li, F.; Evans, D. G.; Duan, X. In situ polymerization of the 4-vinylbenzenesulfonic anion in Ni-Al-layered double hydroxide and its molecular dynamic simulation. *J. Phys. Chem. A* **2008**, *112*, 7671−7681.
(23) Mohanambe, L.; Vasudevan, S. Anionic clays containing anti-inflammatory drug molecules: comparison of molecular dynamics simulation and measurements. *J. Phys. Chem. B* **2005**, *109*, 15651−15658.
(24) Neilson, J. R.; Kurzman, J. A.; Seshadri, R.; Morse, D. E. Cobalt coordination and clustering in α-$Co(OH)_2$ revealed by synchrotron X-ray total scattering. *Chem.—Eur. J.* **2010**, *16*, 9998−10006.
(25) Vialat, P.; Mousty, C.; Taviot-Gueho, C.; Renaudin, G.; Martinez, H.; Dupin, J.-C.; Elkaim, E.; Leroux, F. High-performing monometallic cobalt layered double hydroxide supercapacitor with defined local structure. *Adv. Funct. Mater.* **2014**, *24*, 4831−4842.
(26) Faour, A.; Mousty, C.; Prevot, V.; Devouard, B.; De Roy, A.; Bordet, P.; Elkaim, E.; Taviot-Gueho, C. Correlation among structure, microstructure, and electrochemical properties of NiAl−CO_3 layered double hydroxide thin films. *J. Phys. Chem. C* **2012**, *116*, 15646−15659.
(27) Aimoz, L.; Wieland, E.; Taviot-Guého, C.; Dähn, R.; Vespa, M.; Churakov, S. V. Structural insight into iodide uptake by AFm phases. *Environ. Sci. Technol.* **2012**, *46*, 3874−3881.
(28) Miao, J.; Xue, M.; Itoh, H.; Feng, Q. Hydrothermal synthesis of layered hydroxide zinc benzoate compounds and their exfoliation reactions. *J. Mater. Chem.* **2006**, *16*, 474−480.
(29) Lerf, A. In *Handbook of Nanostructured Materials and Nanotechnology (Intercalation Compounds in Layered Host Lattices: Supramolecular Chemistry in Nanodimensions)*; Nalwa, H. S., Ed.; Academic Press: San Diego, CA, 2000; Vol. *5*: Organics, polymers, and biological materials, pp 1−166.
(30) Fogg, A. M.; Dunn, J. S.; O'Hare, D. Formation of second-stage intermediates in anion-exchange intercalation reactions of the layered double hydroxide $[LiAl_2(OH)_6]Cl{\cdot}H_2O$ as observed by time-resolved, in situ X-ray diffraction. *Chem. Mater.* **1998**, *10*, 356−360.
(31) Du, Y.; O'Hare, D. Observation of staging during intercalation in layered α-cobalt hydroxides: a synthetic and kinetic study. *Inorg. Chem.* **2008**, *47*, 11839−11846.
(32) Iyi, N.; Fujii, K.; Okamoto, K.; Sasaki, T. Factors influencing the hydration of layered double hydroxides (LDHs) and the appearance of an intermediate second staging phase. *Appl. Clay Sci.* **2007**, *35*, 218−227.
(33) Kooli, F.; Chisem, I. C.; Vucelic, M.; Jones, W. Synthesis and properties of terephthalate and benzoate intercalates of Mg-Al layered double hydroxides possessing varying layer charge. *Chem. Mater.* **1996**, *8*, 1969−1977.
(34) *JCPDS PDF-2 Database*; International Centre for Diffraction Data: Newtown Square, PA, 2004.
(35) Whittingham, M.; Jacobson, A. *Intercalation Chemistry*; Academic Press: New York, 1982.
(36) Rodriguz-Carvajal, J. Recent developments in the program FULLPROF. *Newsletter* **2001**, *26*, 12−19.
(37) Qiu, X.; Thompson, J. W.; Billinge, S. J. L. PDFgetX2: a GUI-driven program to obtain the pair distribution function from X-ray powder diffraction data. *J. Appl. Crystallogr.* **2004**, *37*, 678.
(38) Farrow, C. L.; Juhas, P.; Liu, J. W.; Bryndin, D.; Bozin, E. S.; Bloch, J.; Proffen, T.; Billinge, S. J. L. PDFfit2 and PDFgui: computer programs for studying nanostructure in crystals. *J. Phys.: Condens. Matter* **2007**, *19*, 335219.
(39) *Materials Studio Modeling Environment, Release 4.3 Documentation*; Accelrys Software Inc.: San Diego, CA, 2003.
(40) Rappé, A. K.; Goddard, W. A., III. Charge equilibration for molecular dynamics simulations. *J. Phys. Chem.* **1991**, *95*, 3358−3363.

(41) Mayo, S. L.; Olafson, B. D.; Goddard, W. A., III. DREIDING: a generic force field for molecular simulations. *J. Phys. Chem.* **1990**, *94*, 8897−8909.
(42) Karasawa, N.; Goddard, W. A., III. Acceleration of convergence for lattice sums. *J. Phys. Chem.* **1989**, *93*, 7320−7327.
(43) VandeVondele, J.; Krack, M.; Mohamed, F.; Parrinello, M.; Chassaing, T.; Hutter, J. QUICKSTEP: fast and accurate density functional calculations using a mixed Gaussian and plane waves approach. *Comput. Phys. Commun.* **2005**, *167*, 103−128.
(44) Lippert, G.; Hutter, J.; Parrinello, M. A hybrid Gaussian and plane wave density functional scheme. *Mol. Phys.* **1997**, *92*, 477−487.
(45) CP2K version 2.2.426 (Release Version), the CP2K developers group (2011). CP2K is freely available from http://cp2k.berlios.de/.
(46) Becke, A. D. Density-functional exchange-energy approximation with correct asymptotic behavior. *Phys. Rev. A* **1988**, *38*, 3098−3100.
(47) Lee, C.; Yang, W.; Parr, R. G. Development of the Colle-Salvetti correlation-energy formula into functional of the electron density. *Phys. Rev. B* **1988**, *37*, 785−789.
(48) Goedecker, S.; Teter, M.; Hutter, J. Separable dual-space Gaussian pseudopotentials. *Phys. Rev. B* **1996**, *54*, 1703−1710.
(49) Krack, M. Pseudopotentials for H to Kr optimized for gradient-corrected exchange-correlation functionals. *Theor. Chem. Acc.* **2005**, *114*, 145−152.
(50) Zijlstra, E. S.; Huntemann, N.; Kalitsov, A.; Garcia, M. E.; von Barth, U. Optimized Gaussian basis sets for Goedecker-Teter-Hutter pseudopotentials. *Modell. Simul. Mater. Sci. Eng.* **2009**, *17*, 015009.
(51) Cell space filling = occupied volume/total cell volume; free cell volume = 1 − cell space filling.
(52) Inomata, K.; Ogawa, M. Preparation and properties of Mg/Al layered double hydroxide-oleate and -stearate intercalation compounds. *Bull. Chem. Soc. Jpn.* **2006**, *79*, 336−342.